

Computed Tomography-Based Finite Element Model of the Human Thorax for High-Frequency Chest Compression Therapy

Arife Uzundurukan^{1,2}, Sébastien Poncet^{1,2}, Daria Camilla Boffito³, Philippe Micheau^{1,2}

¹Mechanical Engineering Department, Université de Sherbrooke,
2500 Boulevard de l'Université, Sherbrooke, J1K 2R1, Québec, Canada

²Centre de Recherche Acoustique-Signal-Humain, Université de Sherbrooke,
2500 Boulevard de l'Université, Sherbrooke, J1K 2R1, Québec, Canada

Arife.Uzundurukan@Usherbrooke.ca; Sebastien.Poncet@Usherbrooke.ca; Philippe.Micheau@Usherbrooke.ca

³Department of Chemical Engineering, Polytechnique Montréal,
2500 Chemin de Polytechnique, Montréal, H3C 3A7, Québec, Canada
Daria-camilla.Boffito@Polymtl.ca

Abstract - The computed tomography-based finite element model (CT-FEM) is an increasingly promising tool for the numerical optimization of treatments and therapies. This model enables not just only reducing the number of in vivo studies but also increasing their reproducibility. For that reason, CT-FEM is a critical combination in the design and optimization of treatments and therapies. High-frequency chest compression (HFCC) therapy with acoustic devices is one of the most promising techniques in terms of providing efficient and independent therapy for airway clearance. However, puzzling operating frequencies in the literature need to be optimized so patients can get the most out of therapy. In this study, a whole human thorax CT image is transformed into 3D realistic chest geometry to illustrate the HFCC effects on the human chest for airway clearance therapy (ACT). The developed CT-FEM consists of soft tissues, rib cage, lungs, scapula, and trachea. It is created using the chest imaging platform with 8121 faces, 12514 edges, and 4236 points. Moreover, the generated comprehensive, realistic, high-quality, simulation model is tested by FEM and supported by different and independent ACT experimental findings from the literature.

Keywords: 3D imaging, biomedical engineering, chest imaging, biomedical image repairment

1. Introduction

In 2008, the US National Cancer Institute began to build the Quantitative Imaging Network (QIN) initiative to advance quantitative imaging in the context of personalized therapy and the evaluation of treatment response. Image processing applications have been used in areas such as agriculture, finance, engineering, and medicine. Biomedical imaging is a powerful tool for visualizing pulmonary disease diagnoses such as chronic obstructive pulmonary disease (COPD), cystic fibrosis, lung cancer and COVID-19 [1], among other examples. To work with realistic geometry, clinical image processing is crucial to obtain accurate results in 3D analysis. Biomedical imaging is known as an interdisciplinary study, where collaboration among biologists, chemists, medical physicists, pharmacologists, computer scientists, biomedical engineers, and clinicians is vital. Current development tools on the chest imaging platform provide an unprecedented opportunity to use biomedical imaging in finite element models (FEM) for engineering purposes [2,3]. The advantages of such approaches are that they reduce speculation and the risk of human error and minimize variations among individual physicians' abilities. Furthermore, it paves the way for scientists and engineers to do examinations before any in vivo experiment.

COPD is one of the major public health problems worldwide, as it represented the second and the third most common cause of death in terms of the age-standardized death rate in 1990 and 2019, respectively. In order to relieve the symptoms of COPD in the lungs, high-frequency chest compression (HFCC) therapy is applied as an airway clearance therapy (ACT) [3]. However, after the findings of Hansen and Warwick [4], which support HFCC devices that provide 1.8 times higher mucus clearance per therapy session than conventional ones, the popularity of acoustic airway clearance devices (AACD) has skyrocketed.

However, AACDs, based on different principles with different typical frequencies, do not rely on scientific findings. There is no consensus on the resonance frequency of the human thorax. For instance, Goodwin [5] investigated the resonance

frequency for the chest wall as 25 Hz and 33 Hz for 15 healthy male and female volunteers, respectively. Ong and Ghista [6] found the acceleration resonance on average as 27 Hz and 28 Hz for 23 male and female subjects, respectively. However, these results are quite different from the work of McKusick [7]. This last author found that men, women, and children's resonance frequencies were 125 Hz, 150-175 Hz, and 300-400 Hz, respectively.

An accurate Computed Tomography (CT) geometry is necessary to get accurate results from 3D numerical studies, besides the material properties of the respiratory systems [8]. While the necessity of medical imaging in FEM for the optimization of the HFCC cannot be deniable, according to the authors' knowledge, there is not yet any developed whole human thorax model CT-FEM in the literature. Instead of the common patient-specific application in typical imaging studies, the model is developed here based on a CT of an average male patient. Therefore, the present CT-FEM is more general and could enhance our understanding of HFCC by providing more reliable and reproducible results before optimizing the HFCC strategy.

The combination of computed tomography-based finite element model (CT-FEM) and HFCC seems vital to mitigate the puzzling of the resonance frequency, which occurs when a system can store and quickly transfer energy between different storage modes, such as the kinetic energy in a simple pendulum [5,6,9]. Most systems have one resonance frequency and multiple harmonic frequencies with progressively lower amplitudes as they move away from the source [10]. It is a crucial factor in physiotherapy studies [5,6,7]. AACT devices must therefore be designed based on the right value of the resonance frequency of the human thorax to supply the maximum energy with a minimum amplitude for an effective and gentle ACT.

The present study aims at developing a high-quality, comprehensive, and simulation CT-FEM, representative of the average person's features (including soft tissues, rib cage, scapula, lungs, and trachea), to be used in the optimization process of HFCC. Therefore, a series of reparation and simplification methods have been applied to the CT images to get qualified meshes in FEM. The CT visualization is handled by 3D Slicer. For the robustness and accuracy of a biomechanical FEM of a human chest, biomedical imaging is vital. Thus, for repairing, and FreeCAD software is used to make the geometry smoother for 3D analysis using COMSOL in the later stage.

2. Methodology

To create the CT-FEM of the human thorax, the process starts with medical image simulation for soft tissues, rib cage, lungs, trachea, and bronchioles in 3D Slicer, as shown in Fig. 1. Then, the surface number is decreased to create fine surface meshes and get a real geometry from the image.

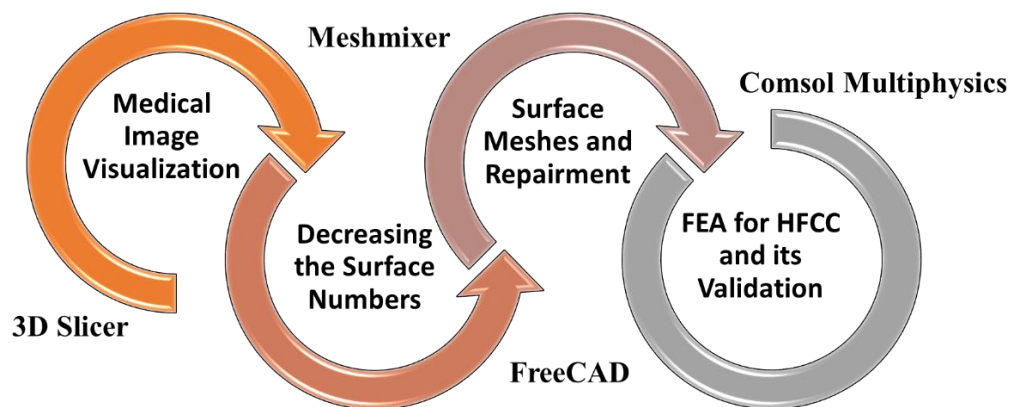


Fig. 1: The methodology of the CT-FEM creation and its validation for HFCC.

2.1. Medical Image Visualization

User interaction is required for reliable segmentation of the chest in clinical practice and clinical research for medical imaging [11]. By incorporating current research tools, 3D Slicer provides a set of interactive, easy-to-use tools that can be efficiently used for this purpose. The use of multiple CT imaging systems is known to result in large

variations, which is especially problematic in multicentre and longitudinal studies [12]. Therefore, in this study, a high-quality example of CT model is used and represents the ideal physical properties of an adult male sample, whose height, weight and chest size are 182 cm, 71.8 kg and 101.9 cm, respectively [13].

CT scans of a thorax usually include different neighbouring internal body organs, so the segmentation of areas in the CT images is vital in computer vision systems in which the pixels of an image are separated into two or more classes to facilitate the upcoming steps [14,15].

Therefore, medical image visualization has been done by "Segment Editor" and "Segment Quantification" in this study. Thresholding is one of the most constant methods that are used to perform this task as it permits having images with high quality according to the level of segmentation [16]. Thresholding-based segmentation is used for the soft tissues, rib cage, scapula, and trachea in a simple, fast, and effective way, thanks to the well-defined densitometric difference. In contrast, slices are used for a proper visualization of the lungs by eliminating the small airway blank geometries [17].

In the segmentation tool, five segments are created, and the first is done with masking. In the mask segment, the threshold ranges between -300 HU and 3071 HU for creating human soft tissues, which contain muscles, skin, and fat.

The created areas are kept as an island in order to create the masking segment. Due to the other organs inside the human torso, open geometries are created automatically. After wiping out the outside spikes, the inside of the mask is entirely filled. After these steps, median smoothing is used to simplify the geometry and to get rid of the spikes. The soft tissues are generated by copying the mask segment using a logical operator tool as shown in Figs 2a to 2c.

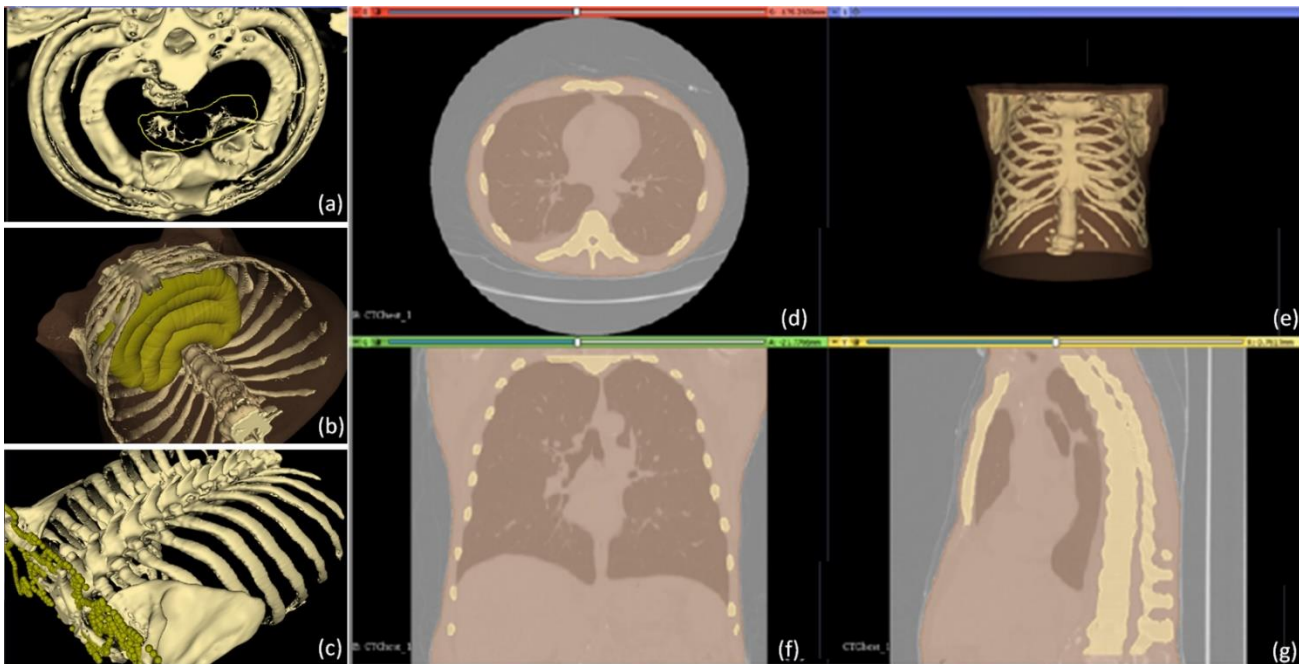


Fig. 2: Illustration of (a-c) the different steps for the manual repair of the rib cage in soft tissues; (d) Axial view, (e) 3D view, (f) coronal view, and (g) sagittal view.

During the creation of the rib cage, the environment is selected as the interior of the soft tissue in order to avoid double lines in the FEM assembly part. The threshold ranges between 135 HU and 3071 HU for the island tool. After the island progressed, many spikes were detected in the geometries. As for the repairment, all low-quality geometries are manually repaired to avoid any detrimental change in the original geometry as shown in Fig. 2.

The lung geometry is determined as being inside the soft tissue environment to avoid double borders and overlapping in FEM. Instead of using thresholding-based segmentation to generate other organs, lungs are created by slices to eliminate the air in the lungs, which can be determined as material properties in FEM.

The interior of the lungs is painted at various locations and regions are contrasted slice by slice. Slices are created by marking different areas of the lungs before generating the lung volume, as shown in Fig.3.

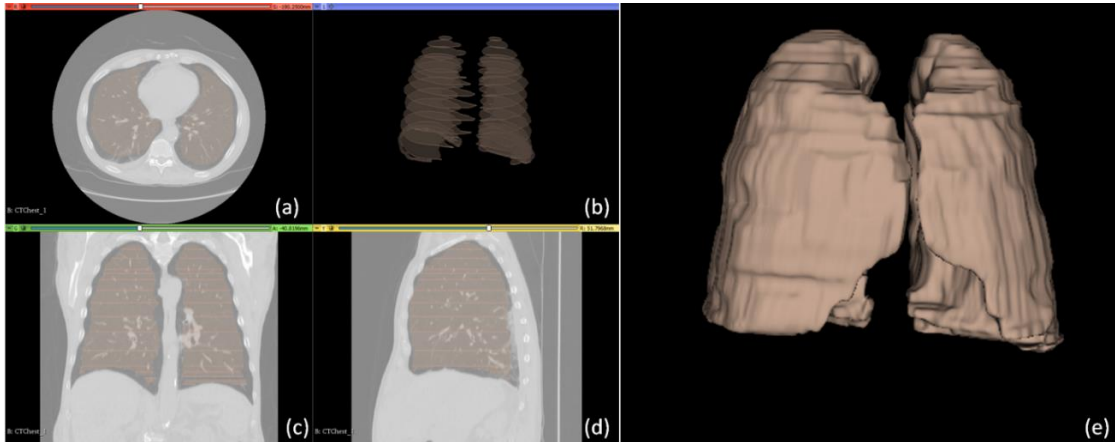


Fig. 3: Generation progress of the human lungs in the four-up window by marking slices in the lungs: (a) axial view, (b) 3D view, (c) coronal view, (d) sagittal view, and (e) 3D view of finalized lung geometry.

In the last segment, the trachea threshold was fixed in the range of -3022 HU and -903 HU in the mask to avoid any overlap when it is transferred to the 3D geometry. During the imaging, extra spike geometries are faced due to the board threshold range of the trachea, and they are then removed. After determining the borders of the trachea, to obtain quality meshes in FEM, the holes are closed as illustrated in Fig. 4.

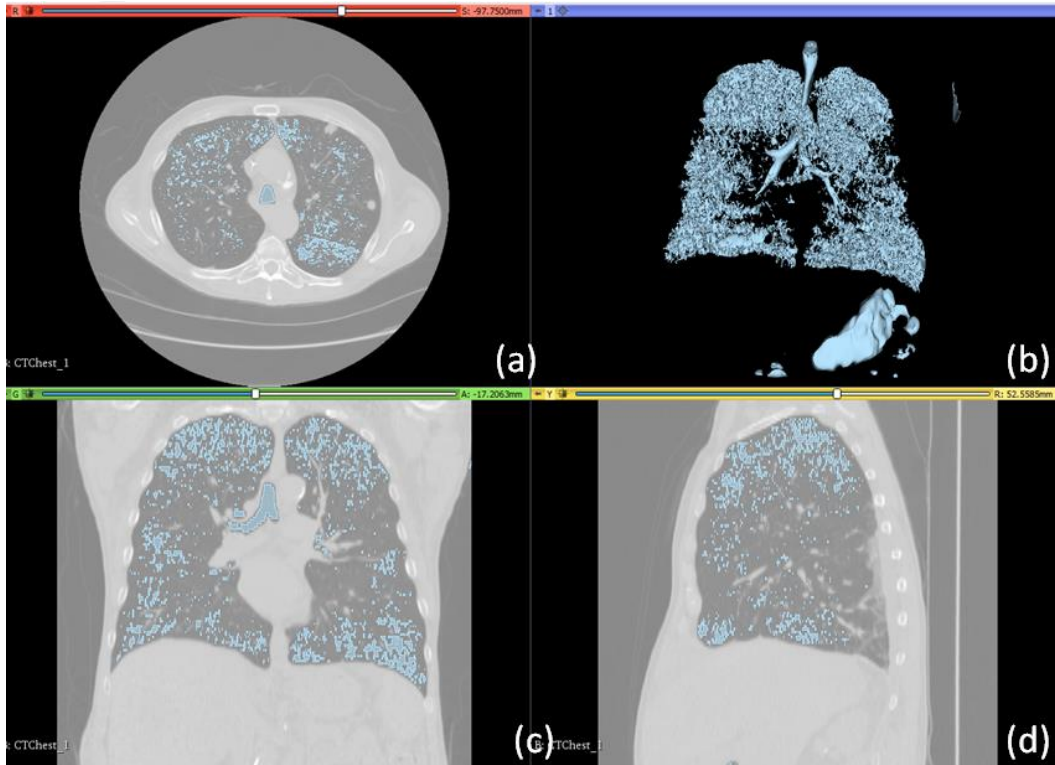


Fig. 4: Created trachea and bronchioles by thresholding in the four-up window: (a) axial view, (b) 3D view, (c) coronal view and (d) sagittal view.

2.2. Image repairment and transformation into a solid geometry

As a first step of the repairment, the geometries were separated to make spike geometries more visible and easily detectable. Then the surface number of each organ was reduced to generate surface meshes for simplification and

having a good mesh quality in FEM. Having a lot of curvature and spikes in the geometries causes difficulties during the meshing progress.

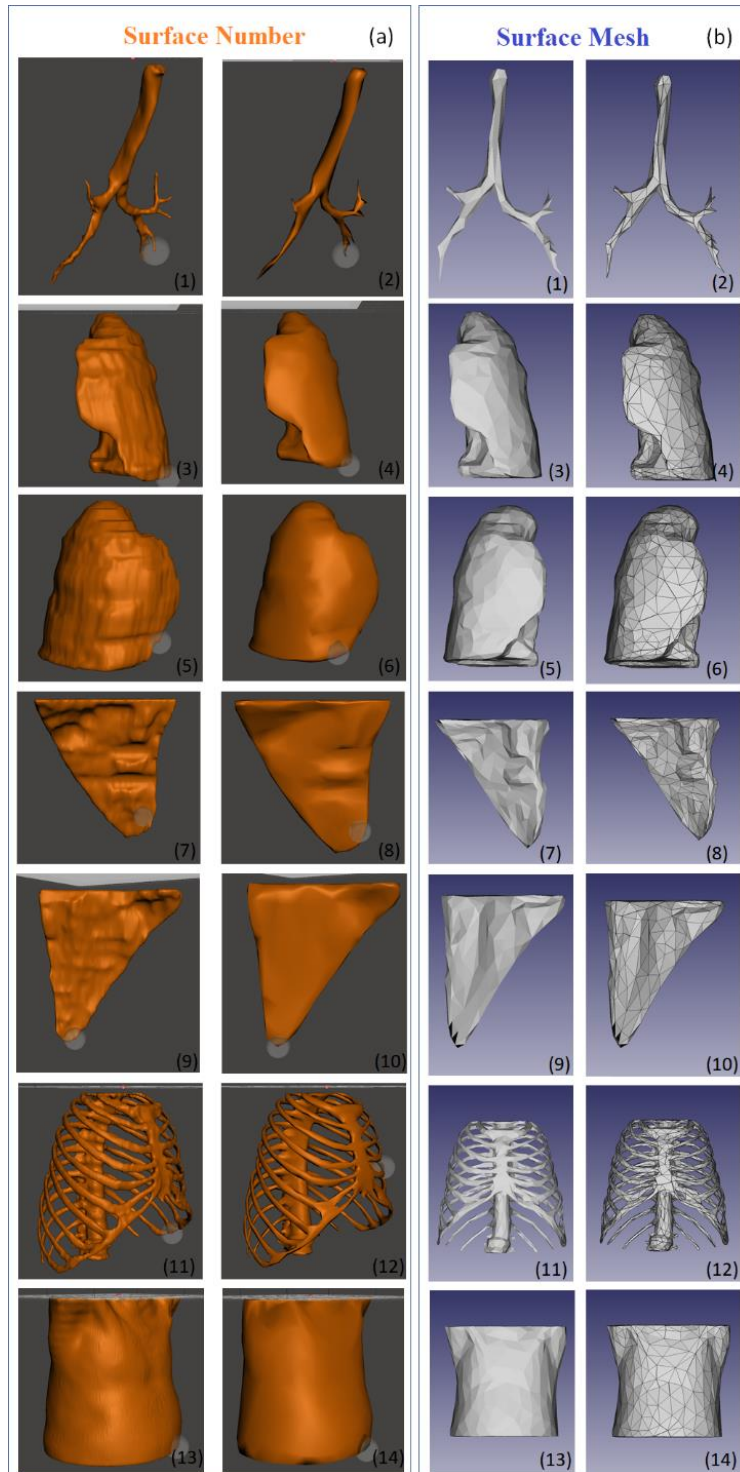


Fig. 5: The geometries before and after decreasing surface and creating solid geometries of (a.1, a.2, b.1, b.2) trachea and bronchioles, (a.3, a.4, b.3, b.4) right lung, (a.5, a.6, b.5, b.6) left lung, (a.7, a.8, b.7, b.8) left scapula, (a.9, a.10, b.9, b.10) right scapula, (a.11, a.12, b.11, b.12), rib cage and (a.13, a.14, b.13, b.14) soft tissues.

The number of surfaces was decreased for the transformation from a surface geometry to a 3D object to generate good quality mesh in 3D CT-FEM. To reach the most accurate geometries, the surface was decreased several times by keeping the shape as constant as possible and checking it in the COMSOL software, as illustrated in Fig. 5a. After decreasing the surface numbers, surface meshes have been created with a tolerance of 0.1 (scale value) when sewing the shape, and the surface geometries have been transformed to actual solid geometries as shown in Fig. 5b. In the mesh module of the software, the created meshes for each of the human organs were tested, evaluated, and repaired in terms of orientation, duplicated faces, duplicated points, nonmanifold, degenerated faces, face indices, self-intersections, and folds on the surface.

Table 1: Number of faces, edges and points in each organ before and after the repairment.

Organs	Before			After		
	Faces	Edges	Points	Faces	Edges	Points
trachea	250	375	127	182	317	117
left lung	1060	1590	532	1060	1590	532
right lung	1075	1615	541	1075	1615	541
left scapula	538	807	271	526	796	269
right scapula	380	570	192	370	559	190
rib cage	4986	7479	2443	4401	6874	2330
soft tissue	510	765	257	507	763	257

For the geometries of each organ, all of the separated geometries were tested, detected, and repaired. The number of faces, edges, and points before and after the repairment progress is given in Table 1 for each organ. The improved faces and edges play a crucial role in the mesh quality of the FEM studies in the computational software. The whole assembled human thorax has a skewness value of 0.5778 with 2999581 tetrahedral elements, 53730 triangles, 32726 edge elements, and 4948 vertex elements, as illustrated in Table 1.

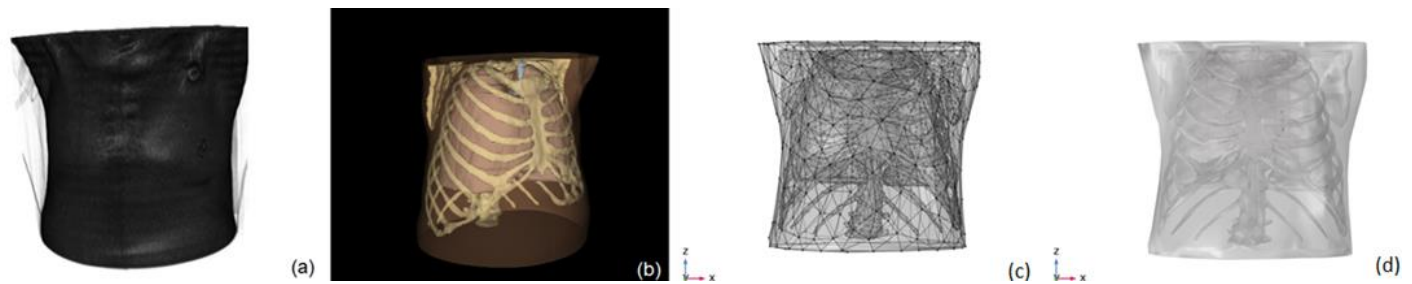


Fig. 6: (a) Medical image, (b) visualization of the internal organs, (c) repairment with surface meshes, and (d) without surface meshes in FEM.

Reparation of the solid geometry of the mesh is deemed necessary for the reproducibility and efficiency of FEM in pulmonary studies. The total number of faces, edges, and points are 8121, 12514, and 4236, respectively, as shown in Table 1. As expected, the lower numbers belong to the smallest geometry, the trachea, while the higher numbers belong to the most prominent geometry that are the soft tissues. The detection of the deteriorated meshes in the rib cage geometry was one of the most challenging part of the reparation due to many spikes and curvature geometries. The medical imaging, the internal organs, and the reparation of the geometry with and without surface meshes in FEM are illustrated in Figs 6a to 6d, respectively.

3. Model validation

As illustrated in Fig. 6d, the created realistic high-quality 3D CT-FEM has been already tested for an HFCC treatment numerically. The material properties of the lungs were calculated using the Biot's theory [18]. For the soft

tissues and osseous region, the material properties were extracted from [19]. During the numerical tests, the low-frequency range was 20 to 60 Hz. The boundary conditions were fixed according to the experiments of [5,6]. A 28 mm radius cylindrical shape section was used to illustrate a shaker on the back-chest surface. The data obtained at the chest surface lead to a peak value at 0.63 m/s^2 for 28 Hz, as shown in Fig. 7b [9].

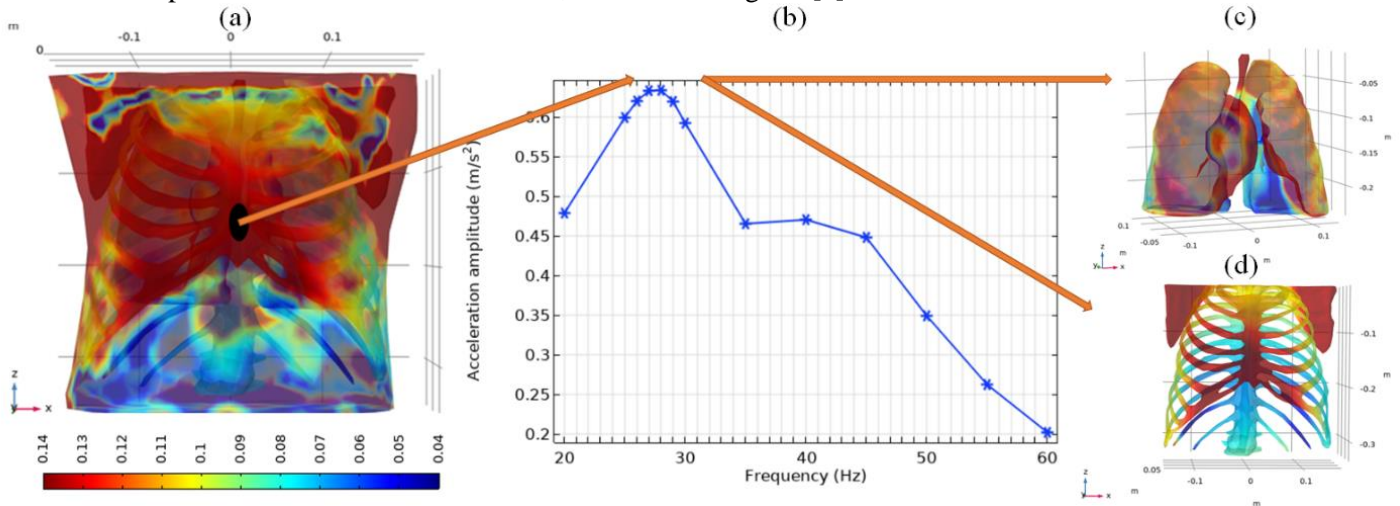


Fig. 7: (a) Illustration of the generated whole thorax, (b) acceleration resonance [9], (c) lungs [2,3] and trachea and (d) rib cage.

The realistic 3D CT-FEM agrees particularly well with the experimental findings of two independent physiotherapy experimental studies. Firstly, Ong and Ghista [6] measured the acceleration resonance as 27 Hz and 28 Hz on average for male and female subjects, respectively, based on a 23-volunteer trial. Secondly, Goodwin [5] found the resonance frequency at 25 Hz for males and 33 Hz for females with a pilot study on a sample of 15 volunteers. The present result is then supported by two independent experimental studies, which increase the reliability of the comprehensive CT-FEM of the human thorax and confirms that it is a powerful model for comprehending the whole thorax under the HFCC effect. Moreover, to go further in ACT with CT-FEM, different tests have been done to see the peak energy density points of the external effects on the lungs and the density distribution at these points [2,3]. However, further analysis is still required to deeply explore the HFCC's impact on internal organs.

4. Conclusion

This paper presented the proper methodology of experimentally supported CT-FEM to develop a comprehensive, high-quality, realistic 3D whole human thorax model consisting of soft tissues, osseous region, lungs and trachea for HFCC therapy. In addition, many repairments and simplification methods, which are essential for mesh quality and computation in engineering, are explained in detail for the realistic 3D human thorax geometry. Furthermore, the created 3D accurate human thorax model has been tested by an acoustic FEM to find the resonance frequency as 28 Hz [9], which matches the values reported by two different and independent experimental physiotherapy studies.

The relationship between HFCC physiotherapy and acoustic numerical studies has been firmly established with such powerful comprehensive CT-FEM. Furthermore, the comprehensive model enables also to investigate the influence of high-frequency vibrations on internal organs, such as the lungs, trachea, and rib cage. In a close future, the model will be extended to quantify the benefit of such a technique on bronchial mucus clearance in the upper airways.

References

- [1] R. Bumm, A. Lasso, N. Kawel-Bohm, A. Wackerlin, P. Ludwig, and M. Furrer, "First results of spatial reconstruction and quantification of COVID-19 chest CT infiltrates using lung CT analyzer and 3D slicer," *British Journal of Surgery*, vol. 108, no. Supplement 4 znab202.077, 2021.
- [2] A. Uzundurukan, S. Poncet, D.C. Boffito, and P. Micheau, "Examination of the behaviour of the lungs under high-frequency chest compression airway clearance therapy," *Proceedings of the Canadian Society for Mechanical Engineering International Congress (CSME 2023) International Congress*, Sherbrooke, QC, CA, 2023.

- [3] A. Uzundurukan, S. Poncet, D.C. Boffito, and P. Micheau, "Numerical analysis of energy density distribution in the human lungs under low-frequency acoustic excitation," *Acoustics Week in Canada*, 2023.
- [4] L. G. Hansen and W.J. Warwick, "High-frequency chest compression system to aid in clearance of mucus from the lung," *Biomedical Instrumentation & Technology*, vol. 24, no. 4, pp. 289–294, 1990.
- [5] M. J. Goodwin, "Measurement of resonant frequencies in the human chest," *Proceedings of the Institution of Mechanical Engineers, Part H: Journal of Engineering in Medicine*, vol. 208, no. 2, pp. 83–89, 1994.
- [6] J. H. Ong and D.N. Ghista, "Applied chest-wall vibration therapy for patients with obstructive lung disease," *Human Respiration: Anatomy and Physiology, Mathematical Modeling, Numerical Simulation and Applications*, vol. 3, pp. 157–167, 2006.
- [7] V. A. McKusick, "The genetic aspects of cardiovascular diseases," *Annals of Internal Medicine*, vol. 49, no. 3, pp. 556–567, 1958.
- [8] S. M. B. Netto, A. C. Silva, R. A. Nunes, and M. Gattass, "Automatic segmentation of lung nodules with growing neural gas and support vector machine," *Computers in Biology and Medicine*, vol. 42, no. 11, pp. 1110–1121, 2012.
- [9] A. Uzundurukan, P. Micheau, S. Poncet, P. Grandjean, and D.C. Boffito, "3D Finite element model of the human thorax to study its low frequency resonance excited by an acoustic harmonic excitation onto the chest wall," *Acoustics Week in Canada*, vol. 49, no. 3, pp. 52–53, 2021.
- [10] D. A. Rice, "Transmission of lung sounds," in *Seminars in respiratory medicine*, *Thieme Medical Publishers, Inc.*, vol. 6, pp. 166–170, 1985.
- [11] S. S. F. Yip, C. Parmar, D. Blezek, R. S. J. Estepar, S. Pieper, J. Kim, and H. J. W. L. Aerts, "Application of the 3D slicer chest imaging platform segmentation algorithm for large lung nodule delineation," *PLoS One*, vol. 12, no. 6, e0178944, 2017.
- [12] E. Benca, M. Amini, and D. H. Pahr, "Effect of CT imaging on the accuracy of the finite element modelling in bone," *European Radiology Experimental*, vol. 4, pp. 1–8, 2020.
- [13] B. Shah, K. Sucher, and C. B. Hollenbeck, "Comparison of ideal body weight equations and published height-weight tables with body mass index tables for healthy adults in the United States," *Nutrition in Clinical Practice*, vol. 21, no. 3, pp. 312–319, 2006.
- [14] A. Tureckov a, T. Turecek, O. Z. Kominkova, and A. Rodriguez-Sanchez, "Improving CT image tumor' segmentation through deep supervision and attentional gates," *Frontiers in Robotics and AI*, 106, vol. 7, pp. 1-14, 2020.
- [15] K. G. Dhal, A. Das, S. Ray, J. Galvez, and S. Das, "Nature-inspired optimization algorithms and their application in multi-thresholding image segmentation," *Archives of Computational Methods in Engineering*, vol. 27, pp. 855–888, 2020.
- [16] F. Chakraborty, P. K. Roy, and D. Nandi, "Oppositional elephant herding optimization with dynamic Cauchy mutation for multilevel image thresholding," *Evolutionary Intelligence*, vol. 12, pp. 445–467, 2019.
- [17] M. Alshipli and N. A. Kabir, "Effect of slice thickness on image noise and diagnostic content of single source-dual energy computed tomography," *Journal of Physics: Conference Series*, vol. 851, 012005, 2017.
- [18] A. Uzundurukan, S. Poncet, D.C. Boffito, and P. Micheau, "The poroviscoelastic model of the lungs under low-frequency predicted by Biot's theory," to be published.
- [19] Z. Dai, Y. Peng, H.A. Mansy, R. H. Sandler, and T. J. Royston, "Comparison of poroviscoelastic models for sound and vibration in the lungs," *Journal of Vibration and Acoustics*, vol. 136, 051012, pp. 1-11, 2014.